MOLECULAR DYNAMICS MODELING OF POLYAMIDE/TITANIUM DIOXIDE NANOCOMPOSITES

M. Salman[1,*], Oday I. Abdullah[2, 3, 4], S. Schmauder[5]

[1]Department of Automated Manufacturing Engineering, Al-Khwarizmi College of Engineering, University of Baghdad, Al-Jadryah, Baghdad, Iraq

[2]College of Engineering, Al-Naji University, Al Yarmouk 10015, Baghdad, Iraq

[3]Department of Energy Engineering, College of Engineering, University of Baghdad, Iraq

[4]Mechanical Engineering Dept., College of Engineering, Gulf University, Bahrain

[5]Institute for Materials Testing, Materials Science and Strength of Materials (IMWF), Universität Stuttgart, Pfaffenwaldring 32, D-70569 Stuttgart, Germany

*Corresponding Author's Email: marwan@kecbu.uobaghdad.edu.iq

Article History: Received 7 January 2026; Revised 30 June 2026; Accepted 4 July 2026

ABSTRACT: Polymer nanocomposites are considered highly applicable materials in a wide range of fields, including industrial, aerospace, and biomedical applications. Understanding the influence of nanoinclusions on the thermomechanical behavior of polymers, particularly at the atomistic scale, provides an important opportunity to improve material performance. In this study, detailed molecular dynamics (MD) simulation models of polyamide 6 (PA6) and PA6/ titanium dioxide (TiO_2) nanocomposites were developed. The study aimed to establish a deeper understanding of material behavior at the atomistic scale and to investigate the interfacial interaction energy between the PA6 matrix and TiO_2 nanoinclusions. In addition, several thermomechanical properties, including Young's modulus, shear modulus, thermal expansion coefficient, glass-transition temperature, and interfacial adhesion energy, were evaluated. The results indicate that the incorporation of TiO_2 nanoinclusions improves the stiffness and mechanical performance of the PA6 matrix, primarily because of more effective load transfer at the PA6/TiO_2 interface. Furthermore, the organic modifier at the interface contributes to interfacial adhesion between the PA6 matrix and TiO_2

nanoinclusions. This work provides valuable insights into the atomistic behavior of PA6/TiO_2 nanocomposites and supports the design and development of high-performance polymer nanocomposites for engineering applications.

KEYWORDS: *polyamide 6; titanium dioxide; molecular dynamics; nanocomposite; atomistic-scale modeling*

1.0 INTRODUCTION

Recently, polymer-based composites have attracted significant attention because of their combination of light weight, tunable properties, and processability, making them suitable for a wide range of functional applications. Polyamide 6 (PA6) has been recognized as one of the most widely used because of its exceptional mechanical properties, chemical resistance, and flexibility. This study demonstrates the effectiveness of molecular dynamics (MD) simulations in investigating the thermomechanical behavior of PA6/titanium dioxide (TiO_2) nanocomposites at the atomistic scale. MD simulations are employed to model the deformation behavior of the material and the influence of TiO_2 reinforcement on the mechanical characteristics of the polymer.

Three different MD models were constructed and evaluated using LAMMPS. The first model explores the mechanical characteristics of pristine PA6 at room temperature. Furthermore, an MD model of PA6/TiO_2 nanocomposites was developed to explore the effects of TiO_2 nanoinclusions on the deformation behavior of the polymer matrix.
Furthermore, extensive research has been conducted on incorporating nanoscale reinforcements to enhance polymer-matrix performance. For instance, Cazan et al. [1] discussed the effects of compositional parameters, such as the surface modification of TiO_2 and the type of polymer matrix, on the thermomechanical characteristics of polymer nanocomposites. Subsequently, Chen et al. [2] conducted coarse-grained molecular dynamics simulations of PA6 to explore the heterogeneous distribution of local stress within the polymer structure. The study found a weak correlation between order parameters and local stress in the PA6 system. Similarly, Pisani et al. [3] investigated the mechanical properties of PA6 reinforced with graphene and carbon nanotubes. In addition, the study focused on the influence of crystallinity and crystal form on material behavior using a multiscale modeling approach. Ikeshima et al. [4] presented a study that

employed MD simulations to investigate the influence of water molecules on the mechanical behavior of PA6 at the atomistic scale. The findings highlighted the importance of water content in determining the mechanical characteristics of the polymer. Subsequently, Krishna et al. [5] enhanced PA6 through the incorporation of nanomilled cellulose. By combining experimental and computational methods, the study provided a detailed understanding of the deformation behavior and interactions between the polymer matrix and cellulose nanoinclusions.

In contrast, Shen et al. [6] examined the effect of nanofiller shape. The study used coarse-grained MD simulations to evaluate spherical and anisotropic rod-like nanoparticles in a polymer matrix. The results showed that nanoparticles with higher aspect ratios provided greater reinforcement than spherical nanoparticles. PA6/silicon carbide (SiC) nanocomposites were fabricated by Qian et al. [7]. The study found that the addition of 5% SiC resulted in a 54% increase in tensile strength and improved fracture toughness by 9.6-fold. Furthermore, the polymer nanocomposites exhibited excellent wear resistance. Similarly, Bazmara et al. [8] developed a numerical study focusing on the functionally graded interphase of nylon 6/clay nanocomposites. They introduced a new approach to estimate the influence of interphase properties on the elastoplastic deformation behavior of nylon 6/clay nanocomposites.

On the other hand, TiO_2 nanoparticles have emerged as effective nanofillers for polymer reinforcement because of their high mechanical strength and large interfacial surface area. Tai et al. [9] explored the mechanical characteristics and molecular structure of polyisoprene/TiO_2 composites using MD simulations. The study focused on the interaction mechanisms between TiO_2 and the polymer matrix. In addition, Shayestehfar et al. [10] investigated the effects of TiO_2 nanoinclusions and microinclusions on the mechanical characteristics of nylon 6. The findings indicated that nanocomposites exhibited higher elongation at break than microcomposites. Rusu et al. [11] used various experimental techniques to characterize the thermal and mechanical characteristics of nylon 6/TiO_2 nanocomposites. The results demonstrated the importance of interfacial adhesion between the nylon 6 matrix and TiO_2 nanofillers for mechanical behavior and thermal stability.

Ou et al. [12] presented a study examining the mechanical characteristics of PA6/functionalized TiO_2 nanocomposites. The study used differential scanning calorimetry (DSC), together with empirical

equations, to estimate crystallization kinetics. The conclusions showed that TiO_2 nanoinclusions acted as nucleating agents and increased the crystallization rate of PA6. Conversely, Dabees et al. [13] explored the thermomechanical performance and tensile-fracture mechanism of PA6 reinforced with TiO_2 and MWCNTs. The study revealed significant interfacial interactions among PA6, TiO_2, and MWCNTs.
The efficiency of stress transfer from the PA6 matrix to the TiO_2 nanofiller is governed by the properties of the interfacial region. Despite the considerable body of experimental work, interfacial interaction mechanisms and their effects on mechanical behavior remain incompletely understood and require molecular-level investigation. Because direct examination of atomic-scale interactions is difficult using conventional experimental techniques, this knowledge gap remains inadequately addressed. MD simulations have emerged as effective computational tools for investigating the mechanical, interfacial, and structural behavior of polymer nanocomposites at the atomistic scale.

In this study, MD simulations were applied to investigate the thermomechanical properties and interfacial behavior of PA6/TiO_2 nanocomposites. The primary objective was to assess the influence of TiO_2 nanofillers on the mechanical and thermal characteristics of the material. In addition, the simulations elucidated the roles of molecular interactions and interfacial adhesion in determining the efficiency of load transfer between the PA6 matrix and TiO_2 nanofillers. The results of this work provide a deeper understanding of polymer–nanoinclusion interfaces and may offer useful guidance for designing next-generation polymer nanocomposites.

2.0 MATERIAL DEFINITION

PA6 is a synthetic polymer composed of repeating units derived from ε-caprolactam (Figure 1). The polymer contains hexamethylene $[-(CH_2)_5-]$ groups connected by amide $(-CONH-)$ linkages. In addition, PA6 exhibits a semicrystalline structure, in which the crystalline phase is stabilized by hydrogen bonding between amide groups.

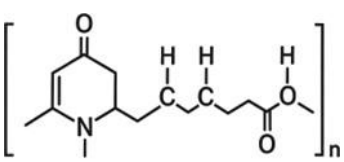

Figure 1: PA6 repeating unit.

Furthermore, TiO_2 is used as a reinforcing nanofiller because of its mechanical and photocatalytic properties. TiO_2 exists in three crystalline phases: rutile, anatase, and brookite. However, rutile is considered the most thermodynamically stable phase and is therefore widely used in polymer nanocomposites. Moreover, TiO_2 has a tetragonal crystal structure, with lattice parameters of a = b = 4.593 Å and c =2.958 Å.

TiO_2 is treated with different organic modifiers to improve interfacial adhesion and dispersion. Silane coupling agents are among the most commonly used modifiers for TiO_2 surfaces [14], [15]. Furthermore, fatty acids have been reported by many research groups to be effective organic modifiers. For example, stearic acid can be used to coat TiO_2 nanoparticles, reducing their agglomeration and promoting the uniform distribution of nanoinclusions throughout the polymer matrix [16], [17].

In addition, carboxylic acid derivatives have been reported in numerous studies as highly effective organic modifiers [18], [19].
Moreover, organophosphonic acids have been reported as common organic modifiers for improving interfacial adhesion in polymer nanocomposites. Specifically, alkylphosphonic acids are used to functionalize TiO_2 surfaces. This modification promotes more effective stress transfer between the PA6 matrix and TiO_2 [20], [21]. In addition, the internal structure of the PA6/TiO_2 system is presented by , as shown in Figure 2.

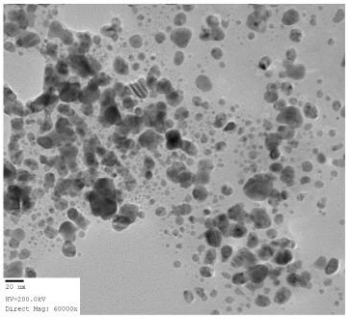

Figure 2: Transmission electron micrograph (TEM) showing the size and distribution of nanoparticles. Adapted with permission from [22].

3.0 MOLECULAR DYNAMICS MODEL SETUP

3.1 COMPASS Force Field

The COMPASS (Condensed-phase Optimized Molecular Potentials for Atomistic Simulation Studies) force field is an all-atom force field with high accuracy that is suitable for simulating a wide range of materials, including polymers, organic materials, and their nanocomposites [23]. In addition to its high accuracy, the COMPASS force field provides an explicit representation of the PA6 polymer matrix, TiO_2 nanoinclusions, and the interfacial interactions between them [24] [25] [26].

The COMPASS force field includes two categories of energy terms: bonded and nonbonded terms. The bonded terms describe intramolecular interactions within the atomic system. They include three interaction components: bond stretching, angle bending, and dihedral torsion. For bond stretching, a harmonic potential is used to characterize the interaction between two atoms according to Equation (1) [27]:

$$E_{bond} = k_b(r - r_0)^2 \tag{1}$$

where k_b is the bond-force constant, r is the distance between the two bonded atoms, and r_0 is the equilibrium bond distance. Similarly, the following harmonic potential defines the angle-bending interaction among three bonded atoms like in Equation (2) [27]:

$$E_{angle} = k_\theta(\theta - \theta_0)^2 \tag{2}$$

where k_θ is the angle-force constant, θ is the angle formed by three bonded atoms, and θ_0 is the equilibrium bond angle. Furthermore, the dihedral torsion energy is represented by the Fourier series in Equation (3) [27]:

$$E_{torsion} = \sum_n k_{\phi,n}(1 + \cos(n\phi - \phi_0)) \tag{3}$$

where $k_{\phi,n}$ is the dihedral torsion constant, ϕ is the dihedral angle, and $\phi_0$is the equilibrium dihedral angle. This energy term governs PA6 chain flexibility and backbone conformation.

In contrast, the nonbonded interaction energy includes electrostatic (Coulombic) and van der Waals interactions. These terms describe intermolecular interactions between the PA6 matrix and TiO_2 nanoinclusions, particularly those influencing interfacial properties. The Coulombic potential is expressed in Equation (4) [27]:

$$E_{elec} = \frac{q_i q_j}{4\pi\epsilon_0 r_{i,j}} \tag{4}$$

where q_i and q_j represent the charges of atom i and atom j, respectively, ϵ_0 is the vacuum permittivity, and $r_{i,j}$ is the distance between the two atoms. Similarly, the repulsive and dispersive interactions are described by the van der Waals potential. The Lennard–Jones 12–6 potential is used to calculate this energy term, as shown in Equation (5) [27]:

$$E_{vdW=}4\varepsilon\left[\left(\frac{r_o}{r}\right)^{12} + \left(\frac{r_o}{r}\right)^{6}\right] \tag{5}$$

where ε represents the depth of the potential well, r_0 is the equilibrium interatomic distance, and r is the interatomic distance.

3.2 Construction of MD Model

The first step in preparing the PA6 molecular dynamics model involved constructing a single PA6 chain using LAMMPS software [28]. The chain was then placed in a simulation box and replicated at random positions and orientations until the model reached a molecular weight representative of bulk PA6. Subsequently, polymerization was initiated by allowing each terminal atom of a PA6 chain to form a new bond with terminal atoms on another chain. To prevent the terminal atoms of PA6 chains from forming bonds with distant chains, a distance criterion of 5 Å was specified in LAMMPS.

The formation of the aforementioned bonds resulted in numerical difficulties, particularly during total-energy minimization. Subsequently, the total energy of the MD model was minimized from 10^6 eV to a range of −5 to 5 eV. Next, the model underwent 50,000 NVE steps at 600 K to promote homogeneous distribution of the PA6 chains within the simulation box. This was followed by 50,000 NPT steps to reduce the temperature of the simulation box to room temperature.

Finally, a 200 × 200 × 200 Å simulation box containing PA6 polymer

chains with a realistic density and an amorphous structure under periodic boundary conditions was prepared for numerical simulations, as shown in Figure 3.

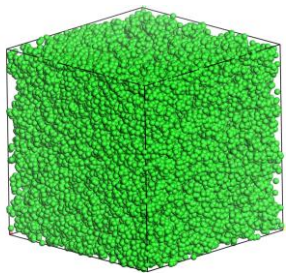

Figure 3: Simulation box containing PA6 polymer chains for MD simulations.

The aim of this research was to investigate the influence of TiO_2 nanocomposites on the thermomechanical properties of the PA6 polymer. An anatase crystal unit was replicated to construct spherical TiO_2 nanoparticles with a diameter of 30 nm, as shown in Figure 4. The prepared nanoparticles were subsequently coated with aminopropyltriethoxysilane organic modifiers. The modified TiO_2 nanoparticles then underwent energy minimization and equilibration, during which the total energy decreased from approximately 10^3eV to a minimum value within the range of −5 to 5 eV.

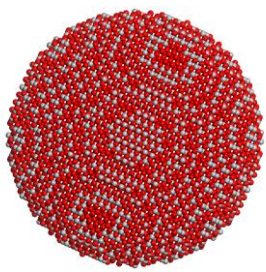

Figure 4: Spherical TiO_2 nanoparticle with a diameter of 30 nm.

The minimized TiO_2 nanoparticle was then inserted into a 500 × 500 × 500 Å simulation box containing PA6 polymer chains, as shown in Figure 5. The simulation box subsequently underwent 50,000 NVE steps to allow the PA6 chains to reorient and form entanglements with the organic-modifier chains. Finally, 50,000 NPT steps were performed to relax the simulation box to a zero-stress state.

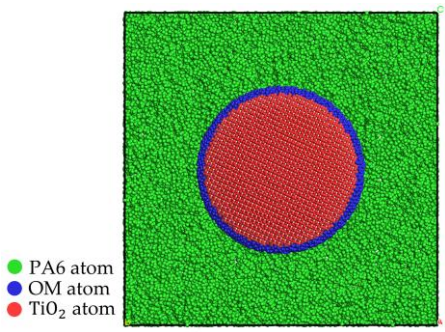

Figure 5: Simulation box of PA6/TiO_2 nanocomposites.

In addition, a simulation box containing three atomic regions was prepared. The first region represents TiO_2 atoms, and the second region represents PA6 atoms. The coupling-agent molecules, aminopropyltriethoxysilane, were positioned between the matrix and TiO_2 nanoinclusions, as also shown in Figure 6.

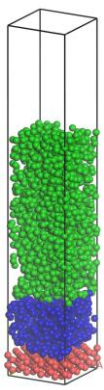

Figure 6: Simulation box containing the three phases of PA6/TiO_2 nanocomposites.

The objective was to estimate the interaction energy among the three material phases and to examine the influence of the organic modifier on interfacial behavior. In addition, energy minimization was performed for the aforementioned system, followed by an NVT equilibration run. The interaction energy was estimated using Equation (6) [28]:

$$E_{interaction} = E_{total} - (E_{PA6} + E_{OM} + E_{NP}) \quad (6)$$

where E_{total} is the total energy of the system, E_{PA6} is the energy of the PA6 component, E_{OM} is the energy of the organic modifier, aminopropyltriethoxysilane, and E_{NP} is the energy of the TiO_2 nanoparticles. Moreover, the work of adhesion, also referred to as

interfacial adhesion energy, was calculated using Equation (7):

$$W_{ad} = \frac{E_{interaction}}{A} \qquad \text{units} \quad J/m^2 \quad \text{or} \quad eV/\text{Å}^2 \tag{7}$$

where A represents the interfacial area.

Within the MD framework, the energy–strain method was used to estimate the elastic properties of the modeled materials. After the atomic structure reached equilibrium, a small strain, ε, was applied to the simulation box. The resulting change in the total energy of the system was estimated using a Taylor-series expansion:

$$\Delta E = E(\varepsilon) - E_0 = \frac{1}{2} V_0 \sum_{i=1}^{6} \sum_{j=1}^{6} C_{ij} \varepsilon_i \varepsilon_j \tag{8}$$

where E_0 is the total energy at the equilibrium configuration, V_0 represents the volume of the simulation box at equilibrium. To estimate Young's modulus, a small strain, ε was applied along the loading direction, and the total energy of the system was calculated. The resulting energy–strain curve was fitted to a quadratic function:

$$E(\varepsilon) = E_0 + a\varepsilon^2 \tag{9}$$

Young's modulus was then calculated as:

$$Young's\ modulus = \frac{2a}{V_0} \tag{10}$$

In contrast, the shear modulus was calculated by applying a small shear strain, γ, to the simulation box. After fitting the corresponding energy changes as a function of shear strain, the shear modulus was calculated from the second derivative of the energy function with respect to shear strain:

$$shear\ modulus = \frac{1}{V_0} \frac{d^2E}{d\gamma^2} \tag{11}$$

Using polynomial fitting, the total energy was expressed as:

$$E(\gamma) = a\gamma^2 \tag{12}$$

The shear modulus was then calculated as:

$$\text{sheer modulus} = \frac{2a}{V_0} \tag{13}$$

Finally, Poisson's ratio was estimated from Young's modulus and the

shear modulus as:

$$\text{Poisson's ratio} = \frac{\text{Young's modulus}}{2*\text{sheer modulus}} - 1 \quad (14)$$

All applied strains were less than 2% to ensure that the system remained within the elastic range and to maintain the validity of the harmonic approximation [29], [30].

4.0 RESULTS AND DISCUSSION

4.1 Mechanical Properties

The mechanical properties evaluated in this study included the elastic stiffness matrix, Young's modulus, shear modulus, and Poisson's ratio for both pristine PA6 and PA6/TiO_2 nanocomposites. All mechanical properties were estimated using the constant-strain method . The PA6 model was examined first. The resulting stiffness matrix, C_{ijkl}, is presented in Figure 7. In addition, the estimated mechanical properties are shown in Figure 8 and compared with experimental results.

$$C_{ijkl} = \begin{bmatrix} 3856 & 1045 & 924 & 0.625 & 0.086 & 0.364 \\ 1045 & 3784 & 937 & 0.402 & 0.117 & 0290 \\ 924 & 937 & 3811 & 0.166 & 0.412 & 0.293 \\ 0.625 & 0.402 & 0.166 & 1231 & 0.168 & 0.271 \\ 0.086 & 0.117 & 0.412 & 0.168 & 1246 & 0.097 \\ 0.364 & 0290 & 0.293 & 0.271 & 0.097 & 1236 \end{bmatrix}$$

Figure 7: Stiffness matrix of the PA6 model.

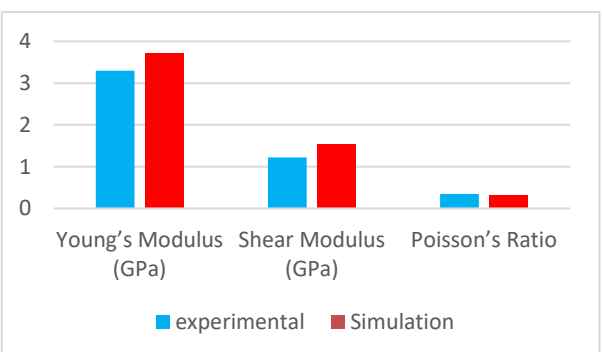

Figure 8: Comparison of simulated and experimental mechanical properties of pristine PA6 [32], [33].

As shown in the results, the simulated values were higher than the experimental values. Such differences are common in MD simulations because the atomistic simulation box represents an idealized material

structure. In particular, material defects present at the macroscale, such as grain boundaries and impurities, cannot be explicitly incorporated into the MD models. Consequently, mechanical properties predicted at the atomistic scale are often higher than those measured experimentally. Nevertheless, the estimated values remain a reasonable approximation of the mechanical properties of the polymer. Similarly, the PA6/TiO_2 nanocomposite model was evaluated using the same method described above. The estimated elastic constants are presented in Figure 9. However, direct comparison of MD-model results with experimental results obtained at the macroscale remains challenging. Alternatively, analytically calculated values can be compared directly with the MD results, as shown in Figure 10. The effect of TiO_2 nanoinclusions within the PA6 matrix on the mechanical properties of PA6 was evaluated using MD simulations.

$$C_{ijkl} = \begin{bmatrix} 5798 & 1708 & 1867 & 0.648 & 0.273 & 0.934 \\ 1708 & 5801 & 1794 & 0.507 & 0.374 & 0268 \\ 1867 & 1794 & 5734 & 0.472 & 0.214 & 0.176 \\ 0.648 & 0.507 & 0.472 & 2869 & 0.634 & 0.819 \\ 0.273 & 0.374 & 0.214 & 0.634 & 2795 & 0.604 \\ 0.934 & 0268 & 0.176 & 0.819 & 0.604 & 2817 \end{bmatrix}$$

Figure 9: Stiffness matrix of the PA6/TiO_2 nanocomposite model.

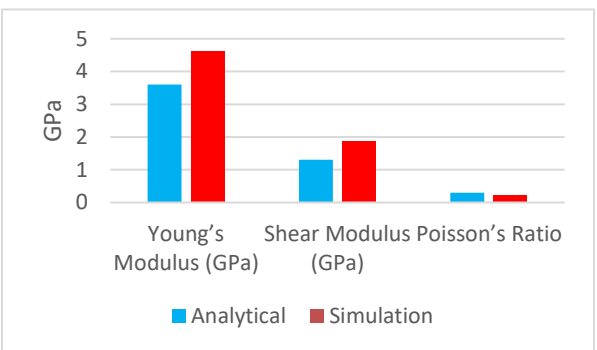

Figure 10: Comparison of simulated and analytical mechanical properties of PA6/TiO_2 nanocomposites.

4.2 Thermal Expansion and Glass-Transition Temperature

Two thermal properties were estimated using MD simulations for both PA6 and PA6/TiO_2 nanocomposites. First, the thermal expansion coefficient was determined by increasing the temperature of the simulation box from 100 K to 600 K and recording the simulation-box volume at different temperatures. The slope of the volume–

temperature curve shown in Figure 11 was used to calculate the thermal expansion coefficient of the simulated materials. Both the PA6 polymer and PA6/TiO_2 nanocomposites were evaluated numerically. Furthermore, the simulation results showed an increase in the thermal expansion coefficient. This increase was attributed to the relatively large difference in thermal expansion coefficients between the PA6 polymer and TiO_2 nanoinclusions.

A sudden change in slope was observed in the volume–temperature curves of both PA6 and PA6/TiO_2 nanocomposites. In addition, each curve exhibited two distinct linear regions with different slopes, separated by the observed transition point. The intersection of these two linear regions represents the glass-transition temperature of the material, as illustrated in Figure 12.

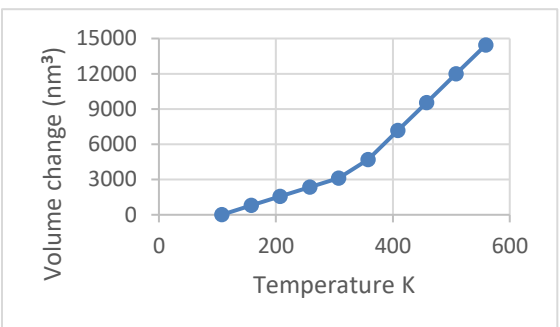

Figure 11: Volume–temperature curve of the PA6 MD model.

The estimated results indicated that the incorporation of TiO_2 as a reinforcement in PA6 improved the thermal properties and thermal stability of the material.

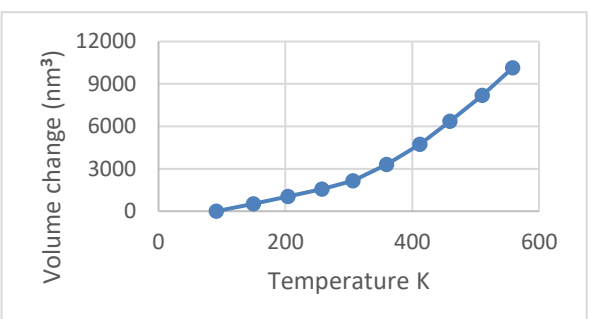

Figure 12: Volume–temperature curve of the PA6/TiO_2 nanocomposite MD model.

This improvement may be attributed to restricted mobility of the PA6 chains in the vicinity of TiO_2 nanoinclusions. Furthermore, the incorporation of TiO_2 nanoinclusions into the PA6 matrix may increase chain entanglement through interactions between PA6 chains and the organic-modifier molecules surrounding the TiO_2 nanoinclusions. As a result, a higher crosslink density may be produced during the polymerization process of PA6. Moreover, TiO_2 nanoinclusions may increase the crystallization rate by acting as nucleating agents, thereby resulting in an increase in the glass-transition temperature, T_g, of PA6/TiO_2 nanocomposites.

5.0 CONCLUSIONS

Reasonable agreement was observed between the simulated and experimental results, supporting the use of the developed MD models for simulations at the atomistic scale. Furthermore, the results showed that incorporating TiO_2 nanoinclusions into the PA6 matrix improved mechanical properties, including tensile strength, Young's modulus, and shear modulus. In addition, organic modifiers surrounding TiO_2 nanoparticles promoted interfacial adhesion between the PA6 matrix and TiO_2 nanoinclusions. Consequently, more efficient load transfer between the PA6 matrix and TiO_2 nanoinclusions was achieved, resulting in a stiffer and stronger nanocomposite structure. In summary, this study provides a deeper understanding of polymer nanocomposite behavior at the atomistic scale. Despite its inherent limitations, the MD approach can provide useful predictions of the thermomechanical properties of polymer nanocomposites that are broadly comparable with experimental results.

REFERENCES

[1] C. Cazan, A. Enesca, and L. Andronic, "Synergic effect of TiO2 filler on the mechanical properties of polymer nanocomposites," *Polymers*, vol. 13, no. 12, p. 2017, 2021.

[2] R. Chen, J. Yang, Z. Ye, and X. Zhang, "Crystallization and Heterogeneous Local Stress Distribution in Hydrogen-Bonded Polymers: Molecular Dynamics Simulations of Polyamide 6 (PA6)," *Macromolecules*, vol. 58, no. 1, pp. 424-438, 2024.

[3] W. A. Pisani, J. L. Rivera, B. D. Jensen, and K. E. Jordan, "Exploration of two polymer nanocomposite structure-property relationships facilitated by molecular dynamics simulation and multiscale modeling," Engineer

Research and Development Center, Vicksburg, MS, USA, Tech. Rep. ERDC TR-23-4, 2023.

[4] D. Ikeshima, F. Nishimori, and A. Yonezu, "Deformation modeling of polyamide 6 and the effect of water content using molecular dynamics simulation," *Journal of Polymer Research*, vol. 26, no. 6, p. 151, 2019.

[5] S. Krishna and C. M. Patel, "Computational and experimental study of mechanical properties of Nylon 6 nanocomposites reinforced with nanomilled cellulose," *Mechanics of Materials*, vol. 143, p. 103318, 2020.

[6] J. Shen, J. Wang, L. Zhang, and X. Li, "Revisiting stress–strain behavior and mechanical reinforcement of polymer nanocomposites from molecular dynamics simulations," *Physical Chemistry Chemical Physics*, vol. 22, no. 29, pp. 16760-16771, 2020.

[7] M. Qian, L. Zhang, Y. Wang, and Z. Chen, "Mechanically robust and abrasion-resistant polymer nanocomposites for potential applications as advanced clearance joints," *Composites Part A: Applied Science and Manufacturing*, vol. 126, p. 105607, 2019.

[8] M. Bazmara, M. Silani, and I. Dayyani, "Effect of functionally-graded interphase on the elasto-plastic behavior of nylon-6/clay nanocomposites; a numerical study," *Defence Technology*, vol. 17, no. 1, pp. 177-184, 2021.

[9] Z. Tai, Y. Chen, X. Liu, and H. Wang, "Molecular dynamics simulation and mechanical properties study of TiO2/polyisoprene composites," *Polymer Composites*, vol. 45, no. 12, pp. 11376-11389, 2024.

[10] S. Shayestehfar, M. Nouri, and A. A. A. Jeddi, "Physical and mechanical properties of nylon 6/titanium dioxide micro and nano-composite multifilament yarns," *Journal of Engineered Fibers and Fabrics*, vol. 9, no. 3, pp. 155892501400900319, 2014.

[11] G. Rusu and E. Rusu, "Anionic nylon 6/TiO2 composite materials: Effects of TiO2 filler on the thermal and mechanical behavior of the composites," *Polymer Composites*, vol. 33, no. 9, pp. 1557-1569, 2012.

[12] B. Ou, D. Li, and Y. Zhang, "Mechanical properties and nonisothermal crystallization kinetics of polyamide 6/functionalized TiO2 nanocomposites," *Polymer Composites*, vol. 35, no. 2, pp. 294-300, 2014.

[13] S. Dabees, T. Osman, and B. M. Kamel, "Mechanical, thermal, and flammability properties of polyamide-6 reinforced with a combination of carbon nanotubes and titanium dioxide for under-the-hood applications," *Journal of Thermoplastic Composite Materials*, vol. 36, no. 4, pp. 1545-1575, 2023.

[14] M. Dinari and A. Haghighi, "Surface modification of TiO2 nanoparticle by three dimensional silane coupling agent and preparation of polyamide/modified-TiO2 nanocomposites for removal of Cr (VI) from aqueous solutions," *Progress in Organic Coatings*, vol. 110, pp. 24-34, 2017.

[15] M. Sabzi, S. M. Mirabedini, J. Zohuriaan-Mehr, and M. Atai, "Surface modification of TiO2 nano-particles with silane coupling agent and investigation of its effect on the properties of polyurethane composite coating," *Progress in Organic Coatings*, vol. 65, no. 2, pp. 222-228, 2009.

[16] H. Masoumi and S. M. Mirfendereski, "Modification of physical and thermal characteristics of stearic acid as a phase change materials using TiO2-nanoparticles," *Thermochimica Acta*, vol. 675, pp. 9-17, 2019.

[17] F. Tang, L. Cao, and G. Fang, "Preparation and thermal properties of stearic acid/titanium dioxide composites as shape-stabilized phase change materials for building thermal energy storage," *Energy and Buildings*, vol. 80, pp. 352-357, 2014.

[18] A. R. Agustin and K. Tamura, "Surface modification of TiO2 nanoparticles with terephthalic acid in supercritical carbon dioxide," *The Journal of Supercritical Fluids*, vol. 174, p. 105245, 2021.

[19] N. Nakayama and T. Hayashi, "Preparation of TiO2 nanoparticles surface-modified by both carboxylic acid and amine: Dispersibility and stabilization in organic solvents," *Colloids and Surfaces A: Physicochemical and Engineering Aspects*, vol. 317, no. 1-3, pp. 543-550, 2008.

[20] P. Chen, L. Wang, and Y. Zhang, "Preparation of polyamide 6 and its titanium dioxide photocatalytic composite powders for laser powder bed fusion," *Materials Science in Additive Manufacturing*, vol. 1, no. 3, p. 14, 2022.

[21] A. Roevens, "In-depth study of organophosphonic acid modification on titanium dioxide," Ph.D. dissertation, Dept. Chem., Univ. of Antwerp, Antwerp, Belgium, 2017.

[22] F. Bano, "Green-synthesized titanium dioxide nanoparticles inhibit and eradicate the biofilms of pathogenic bacteria through intracellular ROS production," *Microbiology Research*, vol. 16, no. 2, p. 48, 2025.

[23] H. Sun, "COMPASS: an ab initio force-field optimized for condensed-phase applications overview with details on alkane and benzene compounds," *The Journal of Physical Chemistry B*, vol. 102, no. 38, pp. 7338-7364, 1998.

[24] T. Zhang, Y. Li, and X. Wang, "Parameterization of a COMPASS force field for single layer blue phosphorene," *Nanotechnology*, vol. 31, no. 14, p. 145702, 2020.

[25] X. Wang, Y. Zhang, and Z. Liu, "Selection of optimal polymerization degree and force field in the molecular dynamics simulation of insulating paper cellulose," *Energies*, vol. 10, no. 9, p. 1377, 2017.

[26] X. P. Chen, Y. Wang, and Z. H. Li, "Validation of forcefields in predicting the physical and thermophysical properties of emeraldine base polyaniline," *Molecular Simulation*, vol. 37, no. 12, pp. 990-996, 2011.

[28] H. Sun, "COMPASS: an ab initio force-field optimized for condensed-phase applications overview with details on alkane and benzene compounds," *The Journal of Physical Chemistry B*, vol. 102, no. 38, pp. 7338-7364, 1998.

[29] A. P. Thompson, H. M. Aktulga, R. Berger, D. S. Bolintineanu, W. M. Brown, P. S. Crozier, P. J. in 't Veld, A. Kohlmeyer, S. G. Plimpton, and F. Pierce, "LAMMPS-a flexible simulation tool for particle-based materials modeling at the atomic, meso, and continuum scales," *Computer Physics Communications*, vol. 271, p. 108171, 2022.

[30] M. Born and K. Huang, *Dynamical Theory of Crystal Lattices*. Oxford, UK: Oxford Univ. Press, 1996.

[31] M. P. Allen and D. J. Tildesley, *Computer Simulation of Liquids*. Oxford, UK: Oxford Univ. Press, 2017.

[32] D. N. Theodorou and U. W. Suter, "Atomistic modeling of mechanical properties of polymeric glasses," *Macromolecules*, vol. 19, no. 1, pp. 139-154, 1986.

[33] P. Song, Y. Zhang, and H. Wang, "Thermomechanical characterisation of polyamide 6 over a wide range of rates and temperatures," *Polymer*, vol. 300, p. 126907, 2024.

[34] M. Dinari and A. Haghighi, "Surface modification of TiO2 nanoparticle by three dimensional silane coupling agent and preparation of polyamide/modified-TiO2 nanocomposites for removal of Cr (VI) from aqueous solutions," *Progress in Organic Coatings*, vol. 110, pp. 24-34, 2017.